RSC Advances

PAPER

Cite this: *RSC Adv.*, 2019, **9**, 30249

Aniline trimer-including carboxymethylated β-cyclodextrin as an efficient corrosion inhibitor for Q235 carbon steel in 1 M HCl solution

Feng Yang,[a] Yu Liu,[ab] Tong Liu,[b] Shuan Liu*[b] and Haichao Zhao *[b]

Received 30th May 2019
Accepted 13th September 2019

DOI: 10.1039/c9ra04047a

rsc.li/rsc-advances

In this work, a water-soluble host–guest complex containing carboxymethylated beta-cyclodextrin (CM-β-CD) and an aniline trimer (AT) was synthesized. The application of AT–CM-β-CD as an inhibitor for alleviating the corrosion of Q235 carbon steel in 1 M HCl solution was investigated by potentiodynamic polarization and electrochemical impedance spectroscopy (EIS). Results showed that the inhibition efficiency was significantly increased in the presence of AT–CM-β-CD, and the inhibition efficiency was up to 99.2% when the concentration of AT–CM-β-CD was 250 mg L^{-1}. Field emission scanning electron microscopy (SEM) and laser scanning confocal microscopy (LSCM) confirmed that the corrosion inhibitor had excellent corrosion inhibition effects due to the formation of an adsorption film on the surface of Q235 carbon steel. According to the data extracted from the Langmuir adsorption model, AT–CM-β-CD absorption involves both physisorption and chemisorption.

1. Introduction

In industry, carbon steel has become the most commonly used construction material in related industries due to its excellent mechanical properties and relatively low price.[1] However, the low resistance of carbon steel to acid corrosion has been a major obstacle for its many applications.[2] Failure of engineering components and premature aging increases maintenance costs and wastes resources. Among the various metal corrosion protection methods, the rational use and addition of corrosion inhibitors is efficient due to simple processes, cost savings and high corrosion inhibition efficiency, and they are widely used in the chemical industry, energy, transportation, *etc.*[3,4]

After continuous exploration by many researchers, conductive polymer materials have been successfully developed into many applications such as metal anti-corrosion, supercapacitors, sensors, and electrochromism, *etc.*[5–8] Initially, conductive polymers (CPs) can be used as corrosion inhibiting additive for organic protective coatings.[9–12] In the 1980s, Mengoli *et al.*[13] and DeBerry.[14] first proposed the possibility of corrosion protection of steel by polyaniline (PANI), which improved the quality of the passivation layer on steel by anodic polarization. PANI is a kind of conductive polymer material with low price and good corrosion resistance. However, the pristine polyaniline has poor solubility either in an organic solvent or aqueous solution, which limited its application as a corrosive inhibitor. Although oligomeric polyaniline such as aniline trimer and tetraaniline showed enhanced solubility in the organic solvent while retaining the similar electrooptical properties of polyaniline, they still suffered from poor solubility in aqueous solution. We have recently synthesized water-soluble quaternary ammonium cation containing tetraaniline with the high inhibition efficiency and adsorption isotherm studies confirmed the adsorption process on Q235 steel surface involved both physisorption and chemisorption.[15] Novel trianiline and polyethylene glycol containing water-soluble polyurethane (TAPU) was also prepared, and potentiodynamic polarization curves showed that the TAPU affected both cathodic and anodic protection and was a mixed type inhibitor.[16]

Cyclodextrin is a cyclic polysaccharide capable of forming host–guest inclusion complexes with appropriately sized hydrophobic molecules or even nanomaterials in aqueous solution.[17–21] carboxymethylated beta-cyclodextrin (CM-β-CD) also has these functions, and its water solubility is greatly improved compared to its unsubstituted analogues. It is utilized as a nano-platform to carry various materials, which can improve the solubility and stability of functional molecules, and also play a sustained release effect. In this work, water-soluble CM-β-CD and aniline trimer (AT) containing host–guest complex AT–CM-β-CD was synthesized as corrosion inhibitor for Q235 carbon steel in HCl solution and the corrosion inhibitive effect on Q235 carbon steel was investigated in HCl medium by using potentiodynamic polarization, scanning electron microscope (SEM) and laser scanning confocal microscope (LSCM) analysis.

[a]*School of Materials Science and Engineering, ShenYang University of Chemical Technology, ShenYang, 110142, China*

[b]*Key Laboratory of Marine Materials and Related Technologies, Zhejiang Key Laboratory of Marine Materials and Protective Technologies, Ningbo Institute of Materials Technology and Engineering, Chinese Academy of Sciences, Ningbo, 315201, China. E-mail: liushuan@nimte.ac.cn; zhaohaichao@nimte.ac.cn*

2. Experimental section

2.1 Materials

Ammonium persulphate, chloroacetic acid, sodium hydroxide, aniline, β-cyclodextrin crystalline (β-CD) were purchased from Aladdin. Ethanol and hydrochloric acid (HCl, 36–38 wt%) were purchased from Sinopharm Chemical Reagent (Shanghai, China). 2 cm × 2 cm × 2 cm Q235 carbon steel was purchased from local suppliers. Deionized water (DI) was used throughout the experiment.

2.2 Synthesis of CM-β-CD

The CM-β-CD was synthesized from a similar report.[22] NaOH (5 g) was dissolved in 120 mL of deionized water, and β-CD (10 g) was added and magnetically stirred until completely dissolved, then 4.2 g of chloroacetic acid in 120 mL deionized water was added dropwise to the mixtures, and kept the reaction react at 60 °C for 5 h. At the end of the reaction, the pH value of the solution was adjusted to 7–8, the CM-β-CD was obtained by precipitation using a large amount of methanol, filtration and drying in an oven at 50 °C for 6 h. Finally, 5.85 g of product was obtained as a powder.

2.3 Synthesis of AT–CM-β-CD

p-Phenylenediamine sulfate (5.2 g), aniline (2.35 g) and CM-β-CD (2 g) was added to 110 mL of 1 M HCl in sequence, and the mixture was kept at 0 °C, after magnetic stirring for 30 min, ammonium persulfate (8 g) in 40 mL of 1 M HCl was added dropwise. The reaction was continued for 1 h after the completion of the dropwise addition, the mixture was then filtered and dried to constant weight under reduced pressure. Finally, 1.96 g of the product was obtained.

2.4 Characterization of AT–CM-β-CD

Fourier transform infrared spectroscopy (FT-IR) was obtained on Nicolai 6700 FT-IR spectrometer. The UV spectrophotometer lambda 950 was used to record the UV-Visible spectrophotometry. TGA measurements were carried out on the Diamond TG/DTA.

2.5 Preparation of electrode and solutions

Q235 carbon steel was polished with 600, 800 and 1000 SiC sandpaper, degreased with alcohol, cleaned by deionized ultrasonic wave, and finally dried at room temperature. Corrosion media were prepared with 1 M HCl solution and AT–CM-β-CD at 50, 100, 150, 200 and 250 mg L^{-1} concentrations. Thirty-six percent of analytical hydrochloric acid was diluted with deionized water to prepare 1 M HCl solution. All tests were carried out at room temperature.

2.6 Electrochemical measurements

Polarization curves and electrochemical impedance spectroscopy (EIS) were analyzed on CHI660E electrochemical station using the traditional three-electrode system. Platinum foil and saturated calomel electrodes were used as counter and reference electrodes respectively. Q235 carbon steel with exposure area of 1 cm^2 was used as working electrode. All tests were carried out at room temperature. Before the test, the open circuit potential test (OCP) was performed for 30 minutes to achieve a stable state. Then EIS is performed on OCP with frequency range of 100 kHz to 10 mHz and interference signal of 10 mV. EIS data were fitted and analyzed by Zsimdemo 3.30d software. Finally, the potentiodynamic polarization test of OCP in the potential range of ±250 mV was carried out at the scanning rate of 5 mV s^{-1}. The same tests were carried out three times to ensure reliability.

2.7 Surface analysis

Laser scanning confocal microscopy (LSCM, LSM700) was used to measure the surface roughness of Q235 carbon steel sample immersed in 250 mg L^{-1} AT–CM-β-CD solution for 3 h. The morphology of Q235 carbon steel immersed in 1 M HCl solution for 3 h was studied by scanning electron microscopy (SEM, Quanta 250) and energy dispersive spectroscopy (EDS).

3. Results and discussion

3.1 Synthesis and characterization of AT–CM-β-CD

Fig. 1 shows the schematic preparation of CM-β-CD and AT–CM-β-CD host–guest complex. As shown in Fig. 2, it was observed that AT–CM-β-CD shows great water solubility compared to pristine AT since AT and CM-β-CD could form supramolecular assembles. This facile water-soluble characteristic is crucial important for initiating its application as inhibitor for alleviating the corrosion of metal in some acidic environments.

Fig. 3 presents the FTIR spectra of CD, CM-β-CD, CD and AT–CM-β-CD. The absorption peak at 3407 cm^{-1} is the –OH absorption peak of β-CD and the C–H peak appears at 2928 cm^{-1}; while the absorption peak intensity of CM-β-CD at 1660 cm^{-1} is significantly enhanced, indicating the presence of C=O absorption peak from a carboxyl substituent.[22] The aniline trimer has a terminal $-NH_2$ characteristic absorption at 3028–3306 cm^{-1}, and the –C=C– stretching vibration of the anthracene ring and the benzene ring at 1603 cm^{-1} and 1502 cm^{-1}, respectively. The absorption peak at 1280 cm^{-1} is –CN stretching vibration, 1145 cm^{-1} is the hydrocarbon stretching vibration in the plane on the benzene ring, and 823 cm^{-1} is the *para*-hydrocarbon bending vibration of the *para*-substituted benzene ring.[23] AT–CM-β-CD is significantly enhanced relative to the AT absorption peak at 2928–3295 cm^{-1} and 1591 cm^{-1}, indicating that the AT–CM-β-CD was successfully synthesized.

Fig. 4 shows the UV-Vis spectra patterns of AT and AT–CM-β-CD. AT displays two main peaks at 295 and 582 nm corresponding to π–π* transition of the benzene ring and the benzenoid to quinoid (π_B–π_Q) excitonic transition, indicating weaker intermolecular interactions.[24] For AT–CM-β-CD, the peaks at 301, 400 and 590 nm are attributed to the π–π* transition, the polaron → π* and π → polaron transitions, which

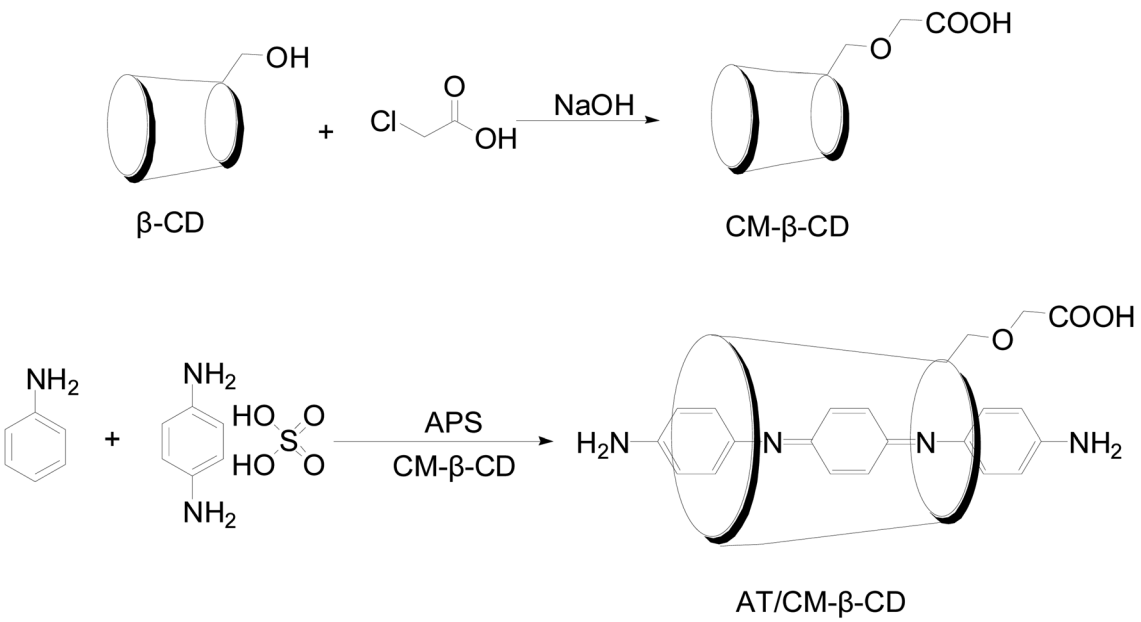

Fig. 1 Schematic preparation of CM-β-CD and AT–CM-β-CD host–guest complex.

demonstrated the formation of conductive state.[24] In addition, this also indirectly illustrates the synthesis of AT–CM-β-CD.

Fig. 5 shows the weight loss of CM-β-CD, AT and AT–CM-β-CD by TGA measurements. The initial weight loss of CM-β-CD, AT and AT–CM-β-CD was observed in the temperature range below 100 °C, which was due to its high hydrophilicity group, resulting in water adsorption in the powder. Clearly, CM-β-CD and AT–CM-β-CD showed significant weight loss regions around 300 °C, which was associated with thermal decomposition of CM-β-CD molecules.[25] AT and AT–CM-β-CD showed weight loss due to thermal decomposition, and we observed multiple thermal degradation processes. The first stage was the decomposition of the amine group (between 250 and 300 °C) and the second stage was the decomposition of the benzene ring (about 400 to 550 °C). Under these conditions, we can conclude that AT and CM-β-CD are successfully complexed to obtain AT–CM-β-CD.

3.2 Potentiodynamic polarization

The potentiodynamic polarization curves of Q235 carbon steel without and with various concentrations of AT–CM-β-CD in 1 M HCl solution are shown in Fig. 6. It can be seen that the polarization plots shift directly to negative potential with the increasing concentration of AT–CM-β-CD. The *i–E* curve was extrapolated to the electrochemical parameter points, including corrosion potential (E_{corr}) and corrosion current density (i_{corr}). These parameters and suppression efficiency are defined as the eqn (1) some parameters are listed in Table 1, the obtained values of η were deduced as follows:[26]

$$\eta\ (\%) = \frac{i_{corr,0} - i_{corr}}{i_{corr,0}} \times 100\% \quad (1)$$

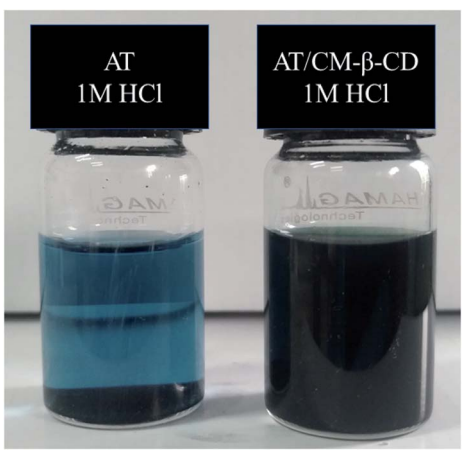

Fig. 2 Photo images of 50 mg L^{-1} of AT and AT–CM-β-CD in 1 M HCl.

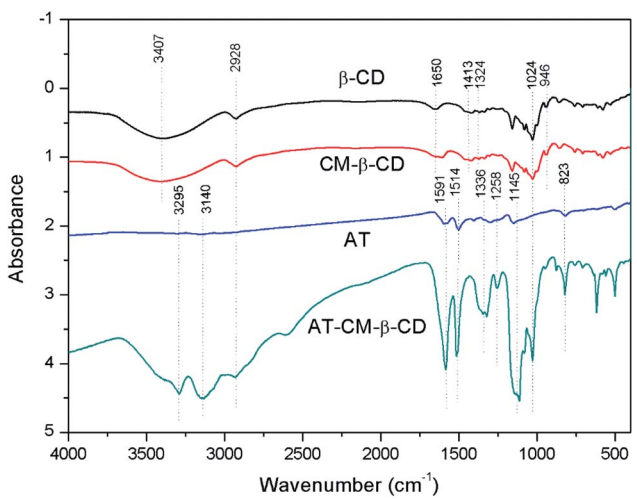

Fig. 3 FTIR of AT–CM-β-CD.

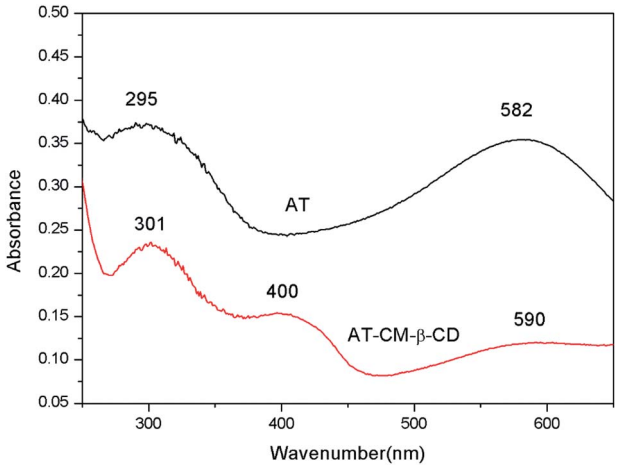

Fig. 4 UV-Vis spectra patterns of AT and AT–CM-β-CD.

where $i_{corr,0}$ and i_{corr} show unprotected and protected current densities of the Q235 carbon steel samples, respectively. As seen in Table 1, the i_{corr} values decreased significantly with the increase of inhibitor concentration, and the values of the inhibition efficiencies are 95.7% for 50 mg L^{-1}, 95.8% for 100 mg L^{-1}, 97.9% for 150 mg L^{-1}, 98.5% for 200 mg L^{-1} and 99.2% for 250 mg L^{-1} of AT–CM-β-CD, respectively. Compared with some work,[27–29] the inhibitor of AT–CM-β-CD have a better inhibition effect on carbon steel.

The results indicated that the β_a value changes significantly in the presence of AT–CM-β-CD, due to the adsorption of chloride ions or inhibitor molecules on the active sites on the metal surface. The change of β_c with the addition of AT–CM-β-CD indicates the effect of the inhibitor on the hydrogen evolution kinetics.[30] Type inhibitors can inhibit anodic dissolution of carbon steel and cathode reduction of H^+.[31] It is apparent that due to the absorption of AT–CM-β-CD on the metal surface, with the i_{corr} decreases, the value of θ and η increase as the concentration of AT–CM-β-CD increases. The lowest i_{corr} values observed for samples immersed in 1 M HCl solution in the presence of 250 mg L^{-1} AT–CM-β-CD were 15.52 μA cm^{-2}, respectively. This result proves that AT–CM-β-CD can be used as an effective corrosion inhibitor for Q235 carbon steel in 1 M HCl solution.

3.3 EIS measurements

In order to obtain the surface characteristics and electrode process kinetics of Q235 carbon steel, the EIS spectra of Q235 in 1 M HCl solution without and with various concentrations of corrosion inhibitors are shown in Fig. 6a–c, and EIS spectra of Q235 steel in 1 M HCl of 250 mg L^{-1} for various immersion time are presented in Fig. 7d–f.

As seen in Fig. 7, for the blank solution, a high frequency (HF) depressed semicircle with its center below the real axis is noticed followed by a straight line at low frequency (LF) range. Generally, the HF semicircle is ascribed to charge transfer resistance and double layer capacitance.[32] For another, LF straight line is related to Warburg impedance due to the diffusion of dissolved oxygen to the Q235 carbon steel surface.[33] The diameter of the curves increases remarkably with addition of all inhibitors compared with the blank solution, indicating high inhibitive ability of these organics. In Fig. 7, the shape of inhibited curves is similar with the uninhibited ones, revealing that the addition of AT–CM-β-CD increase the impedance but did not change the other electrochemical characteristics of the solution due to the relatively looser adsorption films. It is noted that, along with the increasing inhibitor concentration in the solution, the frequency range with the maximum phase angle becomes bigger, showing effective adsorption of inhibitor molecules on the Q235 carbon steel surface.

In Fig. 7a, the diameter of the curves was significantly increased after adding the inhibitors, indicating that AT–CM-β-CD has high inhibition ability. In Fig. 7b and c, the shape of the inhibition curve is similar to the shape of the uninhibited curve, indicating that the addition of AT–CM-β-CD increases the

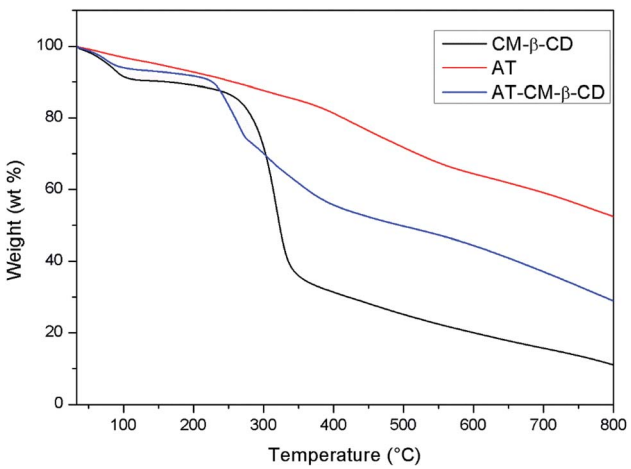

Fig. 5 TGA curves of CM-β-CD, AT and AT–CM-β-CD.

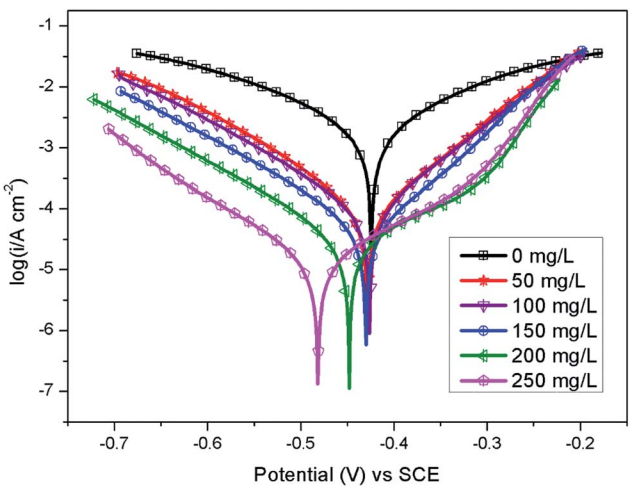

Fig. 6 Tafel curves of Q235 steel without and with various concentrations of AT–CM-β-CD.

Table 1 Corrosion parameters of Q235 steel in various test solutions

C (mg L^{-1})	E_{corr} (mV per SCE)	i_{corr} (μA cm^{-2})	β_c (mV dec^{-1})	β_a (mV dec^{-1})	θ	η (%)
0	−426	2029	−6.74	7.04	—	—
50	−447	87.22	−10	12.43	0.96	95.7
100	−445	83.37	−9.48	11.82	0.96	95.8
150	−423	42.71	−9.34	13.32	0.98	97.9
200	−456	30.64	−9.12	6.882	0.98	98.5
250	−472	15.52	−9.03	7.509	0.99	99.2

impedance but does not alter the other electrochemical properties of the solution due to the relatively loose adsorption film. It is worth noting that the frequency range of maximum phase angle increases with the increase of inhibitor concentration in solution, indicating efficient adsorption of the inhibitor molecule on the surface of the Q235 carbon steel.

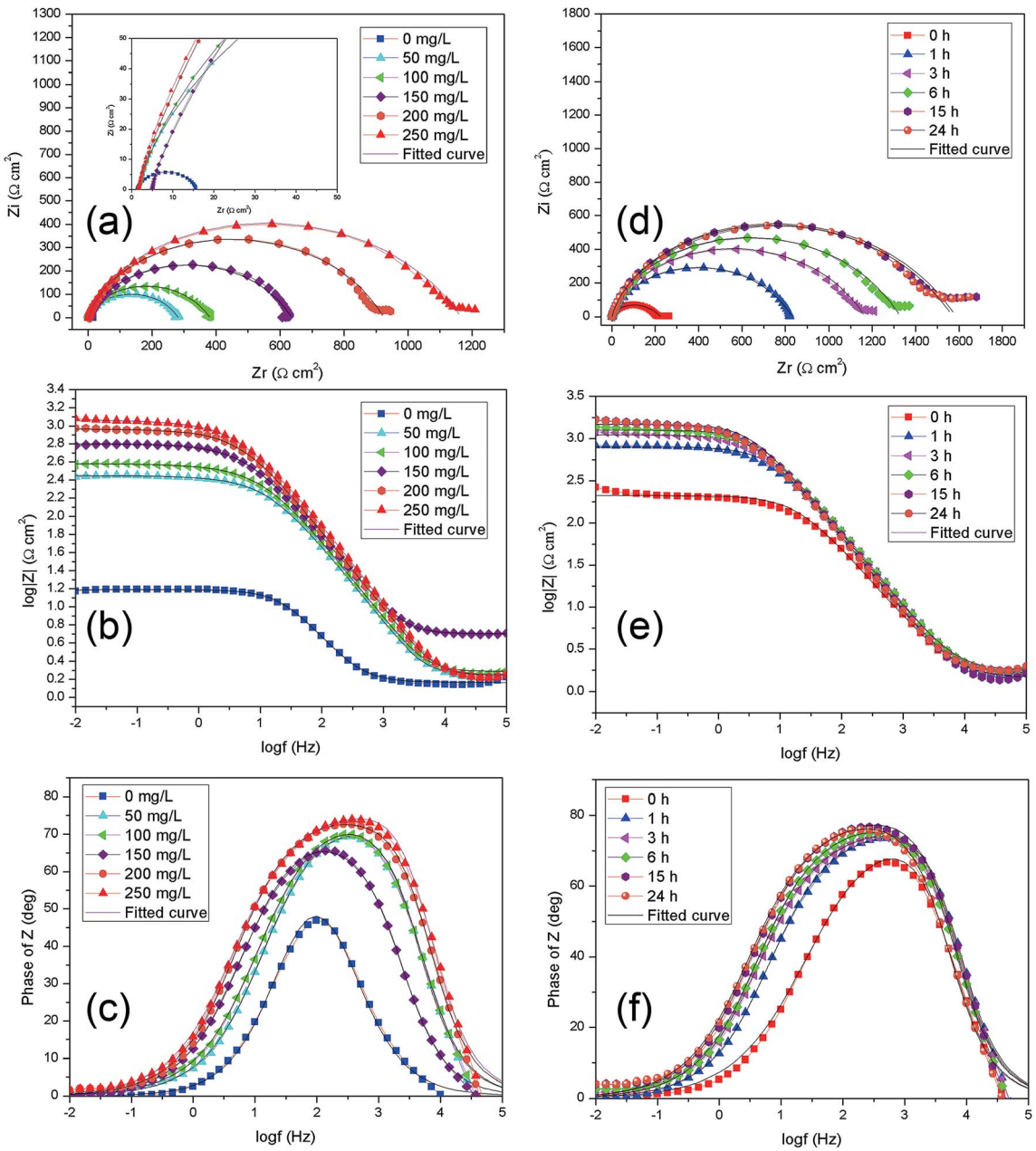

Fig. 7 EIS spectra of Q235 steel in 1 M HCl for various concentrations of AT–CM-β-CD after 3 h immersion (a–c); EIS spectra of Q235 steel in 1 M HCl of 250 mg L^{-1} for various hours immersion (d–f).

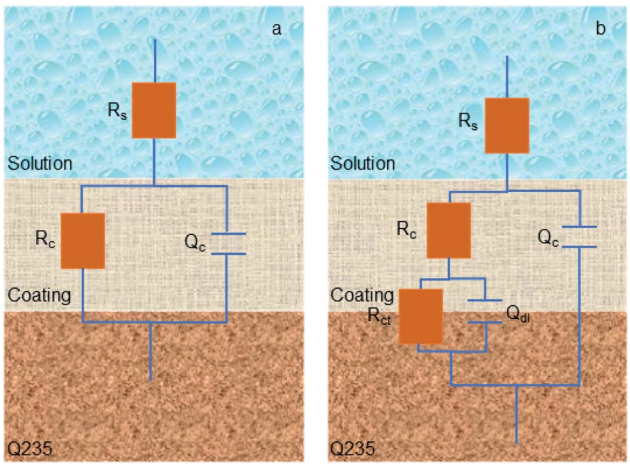

Fig. 8 Equivalent circuit model of corrosion process to fit the EIS results in 1 M HCl solution in the absence of AT–CM-β-CD (a), and in other cases (b).

The effect of immersion time on AT–CM-β-CD corrosion inhibitor was studied. As shown in Fig. 7d–f, the impedance modulus of Q235 carbon steel increased with the immersion time, which confirmed that the corrosion inhibition ability of AT–CM-β-CD exhibited a certain relationship with time. It can be seen from Fig. 7d, that the semicircle radius of capacitor increases with the prolongation of immersion time. This phenomenon may be due to the adsorption of AT–CM-β-CD on carbon steel resulting in the increase of interface impedance, and the film formed by the adsorption of corrosion inhibitor molecules on the surface of steel becomes more denser with time, which plays an excellent protective function.

According to EIS results of all samples, an appropriate equivalent circuit diagram model, such as Fig. 8 is obtained, in the equivalent circuit, R_s, R_c, and R_{ct} correspond to solution resistance, the adsorption layer resistance, and charge transfer resistance, respectively, and the Q_c and Q_{dl} are related to the adsorption layer and the double layer capacitance. The corresponding electrochemical parameters are listed in Table 2. The inhibition efficiency (η) was calculated as follows:[26]

$$\eta\ (\%) = \frac{R_{ct} - R_{ct,0}}{R_{ct}} \times 100\% \quad (2)$$

where R_{ct} and $R_{ct,0}$ are the charge-transfer resistances of Q235 carbon steel with and without investigated organics, respectively. Eventually, the potentiodynamic polarization curve was obtained at a scan rate of 5 mV s^{-1}.

Electrochemical impedance parameters are listed in Table 2. The chi-square (χ^2) test was used to assess the accuracy of the fitted data. Table 2 shows that the χ^2 value is approximately 10^{-3}, indicating that the fitted data agree well with the experimental data. The R_{ct} value increases and the C_{dl} value decreases with the addition of the inhibitor. It can be inferred that the adsorption film formed on the surface of Q235 carbon steel, thus inhibiting the corrosion process.[34–38] As a result, the inhibition efficiency increased with increase of the concentration of inhibitors and reach 94.6% for 50 mg L^{-1}, 96.1% for 100 mg L^{-1}, 97.6% for 150 mg L^{-1}, 98.4% for 200 mg L^{-1}, and 98.8% for 250 mg L^{-1} of the AT–CM-β-CD, respectively. The results show that with the increase of inhibitor concentration, the inhibitor have a better inhibition effect on Q235 carbon steel.

3.4 Surface morphology

As shown in Fig. 9, the scanning electron microscopic images of Q235 carbon steel with or without AT–CM-β-CD were obtained before and after immersion in 1 M HCl solution for 3 hours. The polished Q235 carbon steel is relatively smooth with only some polishing scratches. For Q235 carbon steel immersed in 1 M HCl solution (Fig. 9b), due to severe corrosion damage, its surface is very rough, and there are some pits and cracks. However, in the presence of AT–CM-β-CD (Fig. 9c and d), the corrosion of Q235 carbon steel was significantly inhibited, and the pitting corrosion of Q235 carbon steel surface is less than that of 1 M HCl solution. The results show that the corrosion of Q235 carbon steel in 1 M HCl can be significantly retarded by adding AT–CM-β-CD in a certain concentration range, and the corrosion inhibition effect is better with the increase of concentration.

The EDS spectra and corresponding percentage weight contents are shown in Fig. 10a–d and Table 3. Fig. 10a is an EDS spectrum of Q235 carbon steel in 1 M HCl solution showing C (2.19 wt%), O (5.20 wt%) and Fe (83.46 wt%). For Q235 carbon steel in the presence of 250 mg L^{-1} AT–CM-β-CD in 1 M HCl solution, EDS spectrum C (4.67 wt%), O (2.46 wt%) and Fe (82.66 wt%). However, the EDS spectrum of the 1 M HCl solution in the presence of AT–CM-β-CD was different from the EDS spectrum in the 1 M HCl solution. The decrease in Fe content in the presence of AT–CM-β-CD was 82.66 wt%. These data indicate that the addition of AT–CM-β-CD significantly retards the corrosion of Q235 carbon steel. As shown in the Table 3, after the addition of the prepared AT–CM-β-CD inhibitor, the content of O decreased, the content of N increased. Thereinto, O was derived from the oxide generated during the corrosion process, and N was derived from as-prepared

Table 2 Impedance parameters of Q235 carbon steel in various test solutions

C (mg L^{-1})	R_s (Ω cm^2)	R_c (Ω cm^2)	R_{ct} (Ω cm^2)	C_{dl} (μF cm^{-2})	χ^2 (10^{-3})	η (%)
0	1.46	—	14.02	771.40	14.98	—
50	1.79	19.51	260.90	144.50	10.61	94.6
100	1.95	17.28	363.50	136.10	6.99	96.1
150	5.05	24.52	606.60	99.44	1.39	97.6
200	1.78	25.46	897.90	75.96	7.53	98.4
250	1.73	34.13	1135.00	79.66	6.02	98.8

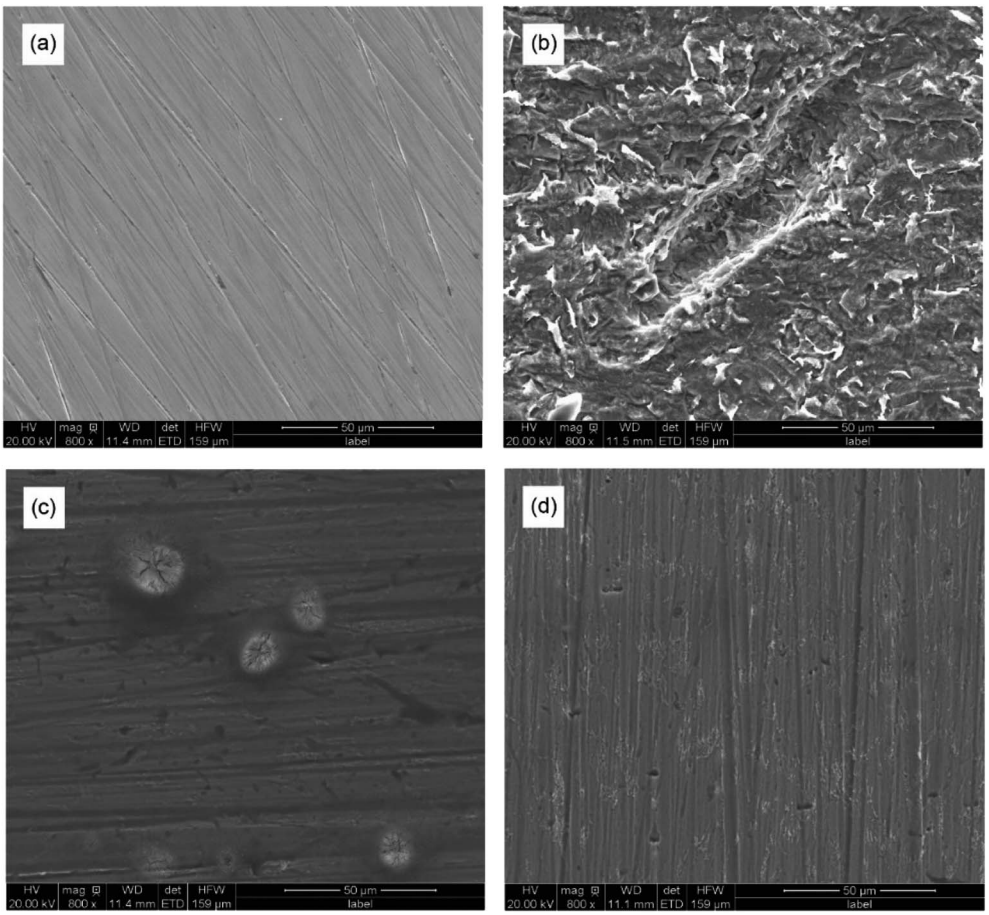

Fig. 9 The SEM images for the polished Q235 carbon steel (a) before and after 3 h of immersion in 1 M HCl solution (b) and in the presence of 50 mg L^{-1} (c) and 250 mg L^{-1} (d) of AT–CM-β-CD.

AT–CM-β-CD inhibitor, indicating that the corrosion inhibitor (AT) adsorbed on the steel surface, which hindered the corrosion reaction of Q235 steel in 1 M HCl.

After immersing for 3 h, the surface roughness (R_a) of Q235 carbon steel was measured by LSCM, as shown in Fig. 11. The polished Q235 carbon steel before impregnation had a R_a value of about 0.21 μm (Fig. 11a). After immersing for 3 hours in 1 M HCl solution, the R_a value of the sample was about 1.06 μm (Fig. 11b). In the presence of 150 mg L^{-1} and 250 mg L^{-1} of AT–CM-β-CD, the R_a values were significantly lower than those in the 1 M HCl solution, which were 0.65 μm and 0.95 μm, respectively (Fig. 11c and d). The results show that the addition of AT–CM-β-CD can inhibit the corrosion of Q235 carbon steel in 1 M HCl solution to some extent, but the corrosion of the sample surface still exists.

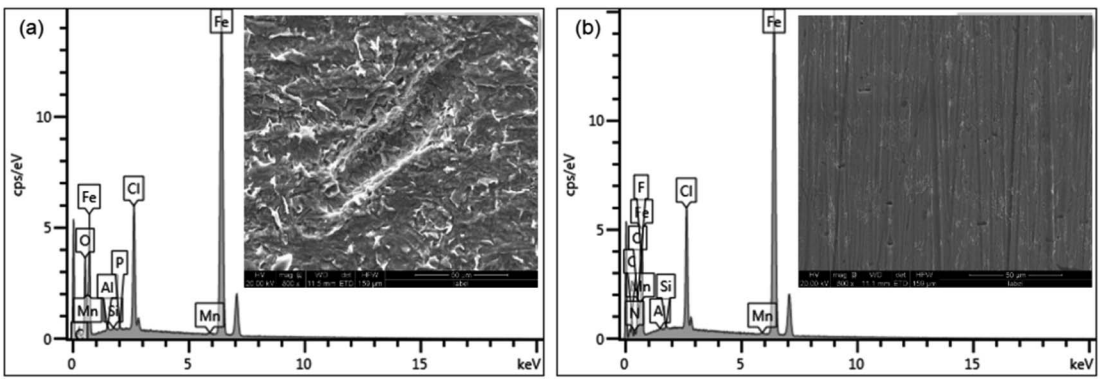

Fig. 10 The EDS spectra of the Q235 carbon steel after 3 h of immersion in 1 M HCl solution in the absence (a) and presence (b) of 250 mg L^{-1} of AT–CM-β-CD.

Table 3 Percentage weight contents of elements obtained from EDS spectra

	C (wt%)	Fe (wt%)	O (wt%)	N (wt%)	Cl (wt%)	Others (wt%)
0 mg L^{-1}	2.19	83.46	5.20	—	8.37	0.78
250 mg L^{-1}	4.67	82.66	2.46	1.03	8.21	0.97

3.5 Adsorption isotherm

In order to further investigate the adsorption mechanism of corrosion inhibitor on Q235 carbon steel/solution interface, the surface coverage was fitted as a function of corrosion inhibitor concentration to obtain the adsorption isotherm of the corrosion inhibitor. The Langmuir isotherm (eqn (3)) was the most suitable model for measuring potentiodynamic polarization, and all linear regression coefficients (R^2) are about 1.[15,39]

$$\frac{\theta}{1-\theta} = K_{ads}C \quad (3)$$

here, θ is defined as the surface coverage, K_{ads} is the equilibrium constant of the adsorption process, and C is the concentration of the compounds.

Fig. 12 shows the plots of C *versus* C/θ yield straight lines with the intercept of $1/K$. The standard adsorption free energy ΔG^0_{ads} can be calculated as follows,[40]

$$\Delta G^0_{ads} = -RT\ln(1000K_{ads}) \quad (4)$$

where R is the molar gas constant and T is the absolute temperature.

Corresponding thermodynamic parameters for the inhibitor are also given in Fig. 12. Usually, a high value of K_{ads} and low value of ΔG^0_{ads} indicate that the inhibitor could be strongly adsorbed on the metal surface, showing a superior inhibitive ability. The values of K_{ads} listed in Fig. 12 follow the order: 50 mg L^{-1} < 100 mg L^{-1} < 150 mg L^{-1} < 200 mg L^{-1} < 250 mg L^{-1}, and inverse trend are obtained for ΔG^0_{ads}. These results reveal that AT–CM-β-CD with suitable concentration

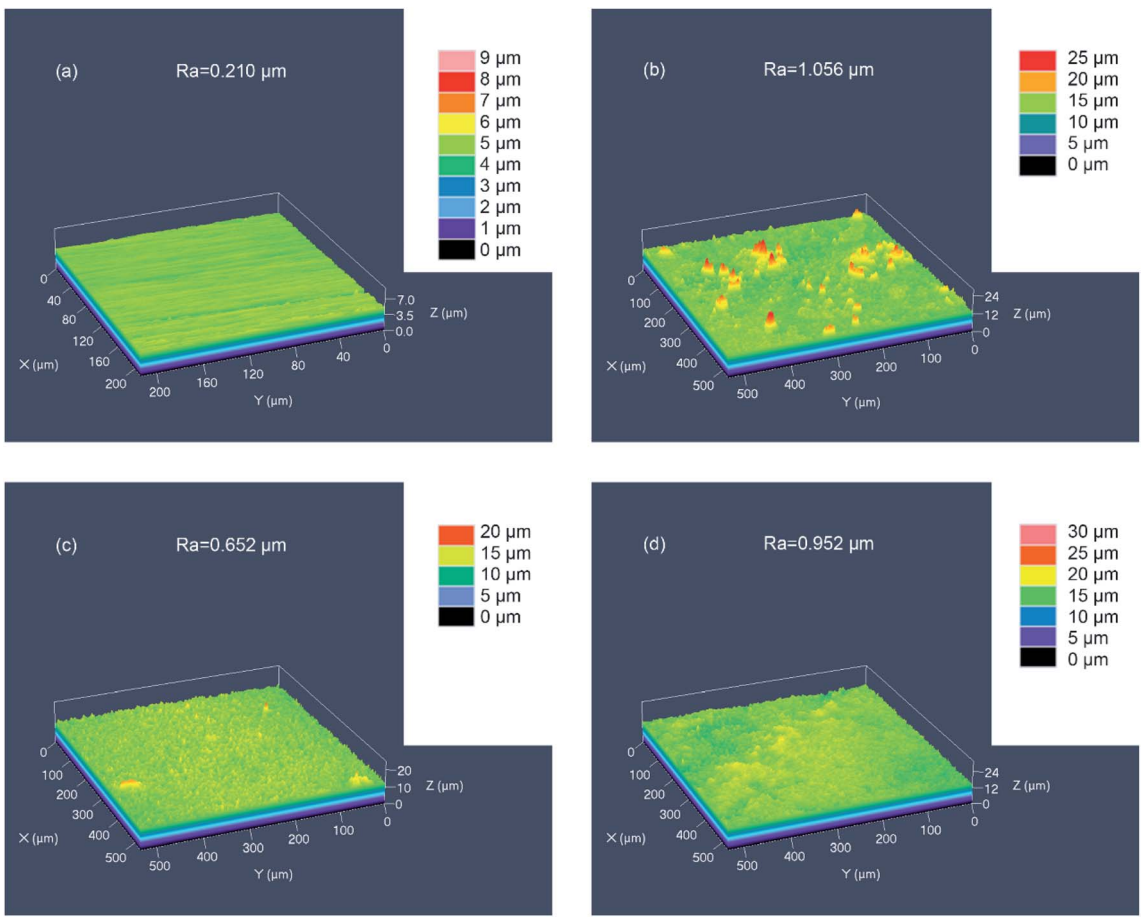

Fig. 11 The surface roughness (R_a) of the polished Q235 carbon steel before (a) and after 3 h of immersion in 1 M HCl solution in the absence (b) and 150 mg L^{-1} (c) and 250 mg L^{-1} (d) of AT–CM-β-CD.

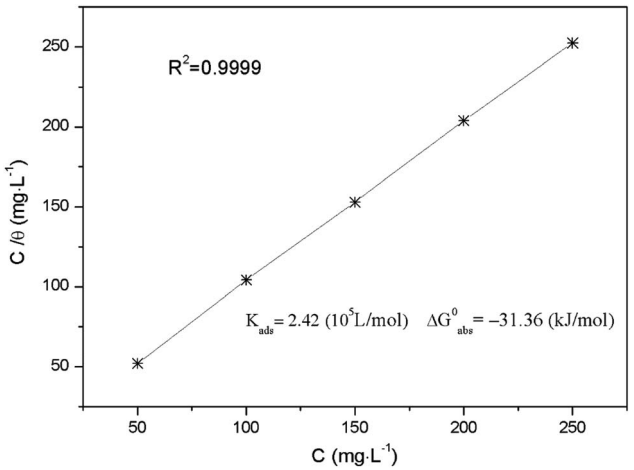

Fig. 12 Langmuir adsorption isotherms of Q235 steel surface in test solutions.

possess stronger adsorption affinity onto the Q235 carbon steel surface, and thus exhibit better inhibition behavior. Typically, the value of ΔG^0_{ads} close to −20 kJ mol^{-1} or less suggests physisorption. The value of ΔG^0_{ads} close to −40 kJ mol^{-1} or more suggests chemisorption.[15] The calculated values of ΔG^0_{ads} is −31.36 kJ mol^{-1}, which means that the study of the interaction between solution and Q235 carbon steel surface suggests both physisorption and chemisorption.[41,42]

4. Conclusions

Novel water-soluble aniline trimer and carboxymethylated β-cyclodextrin based host–guest complex (AT–CM-β-CD) was successfully synthesized, making it possible as corrosion inhibitor for alleviating the corrosion of metal in acidic solution. The polarization curve and EIS results show that AT–CM-β-CD D has an excellent corrosion inhibition effect on Q235 carbon steel in 1 M HCl solutions, and the inhibition efficiency was up to 99.2% when the concentration of AT–CM-β-CD was 250 mg L^{-1}. According to Langmuir adsorption isotherm calculation, the ΔG_{ads} values of Q235 carbon steel in 1 M HCl in presence of AT–CM-β-CD was −31.36 kJ mol^{-1}, indicating that interactions between corrosion inhibitor and Q235 carbon steel surface in 1 M HCl involves both physisorption and chemisorption.

Conflicts of interest

There are no conflicts to declare.

Acknowledgements

The authors gratefully appreciate the financial support provided Zhejiang Province Key Technology Project (2015C01006); "One Hundred Talented People" of the Chinese Academy of Sciences (Y60707WR04); Industrial Major Science and Technology Projects of Ningbo City (Grant No. 2017B10004).

References

1 M. Mobin and M. Rizvi, *Carbohydr. Polym.*, 2017, **156**, 202–214.
2 M. Mobin, M. Rizvi, L. O. Olasunkanmi, *et al.*, *ACS Omega*, 2017, **2**, 3997–4008.
3 S. J. Keny, A. G. Kumbhar, C. Thinaharan, *et al.*, *Corros. Sci.*, 2008, **50**, 411–419.
4 F. Yang and G. Wang, *Nat. Gas Ind.*, 2012, **32**, 94–97.
5 P. P. Deshpande, N. G. Jadhav, V. J. Gelling, *et al.*, *J. Coat. Technol. Res.*, 2014, **11**, 473–494.
6 X. Xia, D. Chao, Z. Fan, *et al.*, *Nano Lett.*, 2014, **14**, 1651–1658.
7 J. F. Fennell, S. F. Liu, J. M. Azzarelli, J. G. Weis, S. Rochat, K. A. Mirica, J. B. Ravnsbæk and T. M. Swager, *Angew. Chem., Int. Ed.*, 2016, **55**, 1266–1281.
8 P. Camurlu, C. Gültekin and V. Gürbulak, *J. Macromol. Sci., Part A: Pure Appl.Chem.*, 2013, **50**, 588–595.
9 S. K. Shukla, M. A. Quraishi and R. Prakash, *Corros. Sci.*, 2008, **50**, 2867–2872.
10 A. A. F. Sabirneeza, S. Subhashini and R. Rajalakshmi, *Mater. Corros.*, 2014, **64**, 74–82.
11 G. G. Wallace, A. Dominis, G. M. Spinks, *et al.*, *ACS Symp. Ser.*, 2003, **843**, 103–123.
12 A. U. Saviour and M. S. Moses, *Prog. Mater. Sci.*, 2019, **104**, 380–450.
13 G. Mengoli, M. T. Munari, P. Bianco, *et al.*, *J. Appl. Polym. Sci.*, 2010, **26**, 4247–4257.
14 D. W. DeBerry, *J. Electrochem. Soc.*, 1985, **132**, 1022.
15 X. Li, Y. Ye, T. Liu, *et al.*, *Surf. Topogr.: Metrol. Prop.*, 2017, **5**, 4.
16 F. Yang, X. Li, S. Qiu, W. Zheng, H. Zhao and L. Wang, *Int. J. Electrochem. Sci.*, 2017, **12**, 5349–5362.
17 A. Popielec, M. Agnes, K. Yannakopoulou, *et al.*, *J. Drug Delivery Sci. Technol.*, 2018, **45**, 20–27.
18 P. Rakkaew, J. Suksiriworapong and D. Chantasart, *Pharm. Dev. Technol.*, 2018, **23**, 715–722.
19 Y. Liu, Y. Liu, Z. Liu, *et al.*, *Anal. Bioanal. Chem.*, 2018, **410**, 509.
20 C. Liu, H. Zhao, P. Hou, B. Qian, X. Wang, C. Guo and L. Wang, *ACS Appl. Mater. Interfaces*, 2018, **10**, 36229–36239.
21 S. Palanisamy, K. Thangavelu, S. M. Chen, *et al.*, *Sens. Actuators, B*, 2017, **243**, 888–894.
22 A. Z. M. Badruddoza, A. S. H. Tay, P. Y. Tan, *et al.*, *J. Hazard. Mater.*, 2011, **185**, 1177–1186.
23 H. Y. Huang, T. C. Huang, J. C. Lin, *et al.*, *Mater. Chem. Phys.*, 2013, **137**, 772–780.
24 Y. Wang, H. D. Tran, L. Liao, *et al.*, *J. Am. Chem. Soc.*, 2010, **132**, 10365–10373.
25 C. Liu, H. Zhao, P. Hou, B. Qian, X. Wang, C. Guo and L. Wang, *ACS Appl. Mater. Interfaces*, 2018, **10**, 36229–36239.
26 A. K. Singh and M. A. Quraishi, *Corros. Sci.*, 2010, **52**, 152–160.
27 P. Kong, H. Feng, N. Chen, *et al.*, *RSC Adv.*, 2019, **16**, 9211–9217.
28 H. S. Gadow and M. M. Motawea, *RSC Adv.*, 2017, **7**, 24576–24588.

29 P. Roy, A. Pal and D. Sukul, *RSC Adv.*, 2014, **21**, 10607.
30 P. Mourya, S. Banerjee and M. M. Singh, *Corros. Sci.*, 2014, **85**, 352–363.
31 M. A. Bedair, M. M. B. El-Sabbah, A. S. Fouda and H. M. Elaryian, *Corros. Sci.*, 2017, **128**, 54–72.
32 L. Hu, S. Zhang, W. Li and B. Hou, *Corros. Sci.*, 2010, **52**, 2891–2896.
33 H. Tian, W. Li and B. Hou, *Corros. Sci.*, 2011, **53**, 3435–3445.
34 X. Zhou, H. Yang and F. Wang, *Corros. Sci.*, 2012, **54**, 200.
35 Sudheer and M. A. Quraishi, *Corros. Sci.*, 2013, **70**, 161–169.
36 R. Solmaz, E. Altunbaş Şahin, A. Döner and G. Kardas, *Corros. Sci.*, 2011, **53**, 3240.
37 Y. Tang, X. P. Guo and G. A. Zhang, *Corros. Sci.*, 2017, **118**, 118–128.
38 Y. Qiang, L. Guo, S. Zhang, *et al.*, *Sci. Rep.*, 2016, **6**, 33305.
39 B. Chugh, A. K. Singh, S. Thakur, B. Pani, A. K. Pandey, H. Lgaz, I.-M. Chung and E. E. Ebenso, *J. Phys. Chem. C*, 2019, **37**, 22897–22917.
40 F. Yang, X. Li, Z. Dai, L. Tong, W. Zheng, H. Zhao and L. Wang, *Int. J. Electrochem. Sci.*, 2017, **12**, 7469–7480.
41 A. Zarrouk, B. Hammouti, A. Dafali, *et al.*, *Ind. Eng. Chem. Res.*, 2013, **52**, 2560–2568.
42 A. Yousefi, S. Javadian and J. Neshati, *Ind. Eng. Chem. Res.*, 2014, **53**, 5475–5489.